Multifractal features of random walks and localized vibrational excitations on random fractals: Dependence on the averaging procedure

Julia Dräger [1,2] and Armin Bunde [1]
[1] *Institut für Theoretische Physik, Justus-Liebig-Universität Giessen, D-35392 Giessen, Germany*
[2] *I. Institut für Theoretische Physik, Universität Hamburg, D-20355 Hamburg, Germany*
(Received 24 June 1996)

We show explicitly that the range of multifractality of random walks and localized vibrational excitations on random fractals depends crucially on the number $N_{\rm av}$ of configurations involved in the averaging procedure. By studying analytically and numerically the moments $\langle P_q(r,t)\rangle_{N_{\rm av}}$ of the probability density of random walks on random walk trails and percolation clusters at criticality, averaged over $N_{\rm av}$ configurations, we find that for fixed distance r and time t multifractality occurs only for q values below a critical value $q_c(N_{\rm av})$ that increases logarithmically with $N_{\rm av}$. We predict similar features for the moments of the amplitudes $\langle \Psi_q(r,\omega)\rangle_{N_{\rm av}}$ of localized vibrational excitations. [S1063-651X(96)08910-6]

PACS number(s): 05.40.+j, 63.50.+x

I. INTRODUCTION

In recent years, it has been shown that several physical quantities describing dynamical properties of random systems do not obey the conventional scaling laws. Recent examples are the electronic eigenstates near the center of the Landau band [1,2], the amplitudes of localized vibrational excitations [3] as well as the probability density of random walks [4] on percolation clusters, and the voltage drops on a bond percolation network [5]. All these quantities have in common that they are characterized by a very broad distribution, such that their moments cannot be described by a single exponent but an infinite hierarchy of exponents is needed to characterize them. This feature is called multifractality (for reviews see, e.g., [6]).

In this paper we mainly concentrate on random walks on random fractals and study both analytically and numerically how the *averaging procedure* influences the multifractal features. We investigate the spatial distribution of random walks on the random fractals by calculating the qth moment $\langle P^q(r,t)\rangle_{N_{\rm av}}$ of the probability to find the random walker, after t time steps, on a site at distance r from its starting point. The average $\langle\ \rangle_{N_{\rm av}}$ is performed over $N_{\rm av}$ configurations.

Previous work on the subject [4] did not consider the role of the averaging procedure. It was suggested that, apart from very small and very large q values, $\langle P^q(r,t)\rangle \sim \langle P(r,t)\rangle^{\tau(q)}$ with

$$\tau(q)\sim q^{\gamma} \quad \text{and} \quad \gamma=\frac{(d_w/d_{\rm min})-1}{(d_w-1)d_{\rm min}}<1. \tag{1}$$

Here, d_w describes how the root mean square displacement of the random walker $\langle R(t)\rangle \sim t^{1/d_w}$ changes with time. The exponent $d_{\rm min}$ is called fractal dimension of the minimum path and describes how the length ℓ of the *shortest path* connecting two points on the fractal (''chemical'' distance) scales with the Euclidean distance r between them, $\langle \ell(r)\rangle \sim r^{d_{\rm min}}$. Similar multifractal features with $\tau(q)\sim q^{1/d_{\rm min}}$ were obtained for the moments of the vibrational amplitudes of localized vibrational excitations (''fractons'') on percolation clusters [3].

Here we show that in both cases the hierarchy of exponents $\tau(q)$ depends explicitly on the number of configurations taken into account in the averages. There exists a critical q value $q_c(N_{\rm av})$ that increases logarithmically with $N_{\rm av}$. Below $q_c(N_{\rm av})$, we find multifractal behavior with $\tau(q)$ from (1). Above $q_c(N_{\rm av})$, we find unifractal behavior, i.e., $\tau(q)=q$. Our considerations include also the case of ''typical'' averages, which formally correspond to $N_{\rm av}=1$, and therefore are described by our analytical results for $N_{\rm av}=1$.

The paper is divided into three parts. In the first part (Sec. II) we discuss random walks on linear fractal structures generated by random walks (RW trails) and test numerically the analytic results, which are rigorous in this case. In Sec. III we extend the approach to random walks on percolation clusters and present numerical simulations for $d=2,3$, and the Cayley-tree. In Sec. IV, finally, we discuss how our results for random walks on random fractals can be applied to localized vibrational excitations on random fractals.

II. RANDOM WALKS ON RW TRAILS

The trace of a random walk in high-dimensional lattices constitutes the simplest random fractal structure with $d_{\rm min}=2$ and $d_w=4$ (see, e.g., [6,7]). Although the trace can intersect with itself in space, only those sites of the trace are considered as connected that have been created sequentially by the random walk. This way the RW trail can be viewed as a topologically linear structure.

We consider a random walker on this structure. The probabilities $P_i(r,t)$ to find a random walker (after t time steps) on sites i at distance r from the starting point of the walk may have very different values. The qth moment, for a given configuration, is defined by

$$P_q(r,t)\equiv\frac{1}{N(r)}\sum_{i=1}^{N(r)} P_i^q(r,t), \tag{2}$$

where $N(r)$ is the number of sites at distance r from the origin of the walk. Along the trail, in ''chemical'' space, the probability of finding the random walker on a site i at ''chemical'' distance ℓ from the origin is (trivially) independent of the considered trail configuration in space and for $t \gg \ell$ given by a Gaussian,

$$P(\ell,t) \sim \exp[-(\ell/L(t))^2], \quad L(t)=\sqrt{2t}. \tag{3}$$

Hence the moments, in chemical ℓ space, are simply

$$P_q(\ell,t) \sim \exp[-q(\ell/L(t))^2] \equiv \exp[-(\ell/L_q(t))^2],$$

$$L_q(t) \equiv L(t)/\sqrt{q}. \tag{4}$$

Assuming that among the $N(r)$ sites at spatial distance r from the origin there are $N(\ell,r)$ sites at chemical distance ℓ, (2) can be written as a sum over sites having the same ℓ values [4,8],

$$P_q(r,t) = \sum_{\ell} \frac{N(\ell,r)}{N(r)} P_q(\ell,t). \tag{5}$$

Averaging over $N_{\rm av}$ configurations and replacing the sum over ℓ by an integral yields the desired relation between the moments of the probability densities in r and in ℓ space (see also [8]),

$$\langle P_q(r,t)\rangle_{N_{\rm av}} = \int_{\ell_{\min}(r,N_{\rm av})}^{\infty} \phi(\ell|r) P_q(\ell,t)\, d\ell. \tag{6}$$

Here $\phi(\ell|r)$ is the probability that two sites at Euclidean distance r from each other are separated by the chemical distance ℓ. The lower integration limit $\ell_{\min}(r,N_{\rm av})$ is defined by $\phi(\ell|r)=0$ for $\ell < \ell_{\min}(r,N_{\rm av})$. For RW trails $\phi(\ell|r)$ can be determined analytically, for $\ell \gg r$,

$$\phi(\ell|r) = \sqrt{\frac{d}{2\pi}} \ell^{-1} \left(\frac{r}{\sqrt{\ell}}\right) \exp\left[-\frac{d}{2}\left(\frac{r}{\sqrt{\ell}}\right)^2\right]. \tag{7}$$

The lower limit $\ell_{\min}(r,N_{\rm av})$ denotes the smallest ℓ value one can find at distance r from the origin in a set of $N_{\rm av}$ configurations. We have found earlier that $\ell_{\min}(r,N_{\rm av})$ scales as [8]

$$\ell_{\min}(r,N_{\rm av}) \sim \begin{cases} r_c(N_{\rm av})^{-1} r^2, & r \gg r_c(N_{\rm av}), \\ r, & r \ll r_c(N_{\rm av}), \end{cases} \tag{8}$$

with the crossover distance

$$r_c(N_{\rm av}) = 1 + \ln N_{\rm av}/\ln z, \tag{9}$$

and z is the coordination number of the underlying lattice.

Now we are in the position to determine the moments $\langle P_q(r,t)\rangle_{N_{\rm av}}$. By substituting (4) and (7) into (6) we can express $\langle P_q(r,t)\rangle_{N_{\rm av}}$ by the first moment $\langle P(r,t)\rangle_{N_{\rm av}}$, according to

$$\langle P_q(r,t)\rangle_{N_{\rm av}} \sim \langle P(rq^{1/4},t)\rangle_{N_{\rm av}}. \tag{10}$$

The first moment $\langle P(r,t)\rangle_{N_{\rm av}}$ has been calculated recently [8,9]. It has been found that the asymptotic regime $r \gg R(t)$ we are interested in is split into two different r regimes that are separated by the crossover distance $r_\times(N_{\rm av}) \simeq R(t) r_c^{3/4}(N_{\rm av})$, with

$$R(t) = \left[L(t) \left(\frac{d}{4}\right)^{1/2} \right]^{1/2} \tag{11}$$

being proportional to the root mean square displacement of the random walker. For $R(t) \ll r \ll r_\times(N_{\rm av})$, the integrand of (6) shows a steep maximum and the method of steepest descent is applicable to calculate the integral (6). One obtains [4,8]

$$-\ln\langle P(r,t)\rangle_{N_{\rm av}} \sim (r/R(t))^{4/3}, \quad R(t) \ll r \ll r_\times(N_{\rm av}). \tag{12}$$

For $r \gg r_\times(N_{\rm av})$, the integrand of (6) is peaked sharply at $\ell_{\min}(r,N_{\rm av})$ yielding [8]

$$-\ln\langle P(r,t)\rangle_{N_{\rm av}} \sim r_c(N_{\rm av})^{-2} (r/R(t))^4, \quad r \gg r_\times(N_{\rm av}). \tag{13}$$

Equations (12) and (13) can be combined into [10]

$$-\ln\langle P(r,t)\rangle_{N_{\rm av}} \sim r_\times(N_{\rm av})^{4/3} f(r/r_\times(N_{\rm av})), \tag{14}$$

with $f(x)=x^{4/3}$ for $x \ll 1$ and $f(x)=x^4$ for $x \gg 1$. From (10), (12), and (13) we can obtain the moments $\langle P_q(r,t)\rangle_{N_{\rm av}}$ when substituting r by $rq^{1/4}$. This yields, for $r \gg R(t)/q^{1/4}$, the more general scaling relation

$$-\ln\langle P_q(r,t)\rangle_{N_{\rm av}} \sim r_\times(N_{\rm av})^{4/3} f(rq^{1/4}/r_\times(N_{\rm av})). \tag{15}$$

Combining (10), (12), and (13), we obtain

$$\langle P_q(r,t)\rangle_{N_{\rm av}} \sim \langle P(r,t)\rangle_{N_{\rm av}}^{\tau(q)} \tag{16}$$

with

$$\tau(q) = \begin{cases} q^{1/3}, & q_1 \ll q \ll q_c(N_{\rm av}) \\ q, & q \gg q_c(N_{\rm av}) \end{cases} \tag{17}$$

and the crossover values

$$q_1 = [R(t)/r]^4, \tag{18}$$

$$q_c(N_{\rm av}) \simeq r_c(N_{\rm av})^3 q_1, \tag{19}$$

and $r_c(N_{\rm av})$ from (9). By definition (17) holds only for $rq^{1/4} \gg R(t)$. For $rq^{1/4} \ll R(t)$, $\tau(q)$ cannot be defined since $\langle P(r,t)\rangle_{N_{\rm av}}$ shows power law behavior for $r \ll R(t)$ [9]. In the limit of $N_{\rm av} \to \infty$, $q_c(N_{\rm av})$ tends to infinity and $\tau(q) \sim q^{1/3}$ reduces to the known result, see (1), in the whole q regime above q_1. For finite $N_{\rm av}$, $\tau(q)$ changes from $q^{1/3}$ to q at $q_c(N_{\rm av})$ and multifractality breaks down. This transition point from multifractal to unifractal behavior increases logarithmically with the number $N_{\rm av}$ of configurations averaged. For $N_{\rm av}=1$, $r_c(N_{\rm av})=1$ and $q_c(N_{\rm av}=1)=q_1$, i.e., we have unifractal behavior in the whole q range above q_1. Recently we have argued theoretically and shown by extensive numerical simulations [10] that the decay of the ''typical'' average $\langle P(r,t)\rangle_{\rm typ} \equiv \exp\langle \ln P(r,t)\rangle$ does not depend on $N_{\rm av}$ and

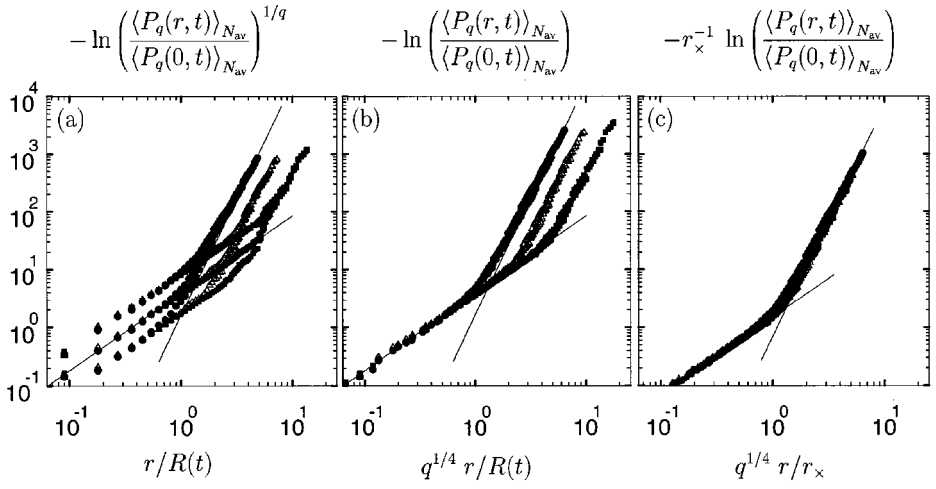

FIG. 1. The logarithm of the averaged moments of the probability density of random walks on RW trails in the s.c. lattice in appropriately scaled form at $t=5000$ (a) as a function of $r/R(t)$, (b) as a function of the single scaled variable $q^{1/4}r/R(t)$, and (c) as a function of the double scaled variable $q^{1/4}r/r_\times(N_{\rm av})$. The different symbols represent the numbers $N_{\rm av}$ of configurations in the averages [$N_{\rm av}=1$ (circles), corresponding to the typical moment, $N_{\rm av}=10$ (triangles), and $N_{\rm av}=10^4$ (squares)]. For each $N_{\rm av}$ three different q values are plotted ($q=0.3$ [upper curve in (a)], $q=1$ [middle curve in (a)], and $q=3.0$ [lower curve in (a)]). The two lines in the plots represent the theoretical slopes 4/3 and 4. For $N_{\rm av}$ below 10^4, averages have been performed over 1000 sets of $N_{\rm av}$ configurations (see also [11]).

is described by Eqs. (12) and (13) with $N_{\rm av}=1$. We can argue (and have verified this by numerical simulations) that also the behavior of $\langle P_q(r,t)\rangle_{\rm typ}\equiv\exp\langle\ln P_q(r,t)\rangle$ is governed by Eqs. (16)–(19) with $N_{\rm av}=1$. Accordingly Eqs. (16)–(19) imply that the multifractal characterization for $rq^{1/4}\gg R(t)$ depends crucially on the averaging procedure. For the typical average, the moments show unifractal behavior, while for the annealed average they are fully characterized by multifractal behavior. We like to note that this typical average must be distinguished from the more conventional ''quenched'' average, where $\ln P_i(r,t)$ is averaged over all sites at distance r and over all cluster configurations [3]. By definition, since $\ln P_i^q=q\ln P_i$, the moments of the quenched average are unifractal in the whole q regime, also for $q<q_1$. In contrast, the typical average is obtained by first averaging $P_i(r,t)$ within one configuration [yielding $P(r,t)$], and *then* averaging $\ln P(r,t)$ over all configurations considered. This way, the fluctuations between different configurations are suppressed, and the result is typical for one individual configuration.

To test our theoretical predictions, we have performed extensive numerical simulations, employing quadruple precision for the data [11]. Figure 1 shows the moments in appropriately scaled form for $t=5000$ and several q and $N_{\rm av}$ values (a) as a function of $r/R(t)$, (b) as a function of the single scaled variable $q^{1/4}r/R(t)$, and (c) as a function of the double scaled variable $q^{1/4}r/r_\times(N_{\rm av})$. The results are in full quantitative agreement with the theory. Figure 2 shows $\tau(q)$ obtained from the moments at fixed r and t value for several values of $N_{\rm av}$. For the typical average corresponding to $N_{\rm av}=1$, there exists only the unifractal region. For $N_{\rm av}\gg 1$, the figure shows clearly the transition from multifractal to unifractal behavior. The transition point $q_c(N_{\rm av})$ increases logarithmically with $N_{\rm av}$, as predicted by the theory.

The above results are rigorous for random walks on RW trails and can be extended straightforwardly to other linear fractals like self-avoiding walks.

III. RANDOM WALKS ON PERCOLATION CLUSTERS

Next we apply the analogous arguments to the more complicated case of random walks on percolation clusters. We shall consider explicitly percolation in $d=2$ ($d_{\rm min}\simeq 1.13$, $d_w\simeq 2.87$), in $d=3$ ($d_{\rm min}\simeq 1.37$, $d_w\simeq 3.8$) [6], and on the Cayley-tree ($d_{\rm min}=2$, $d_w=6$). As above, we define the chemical distance ℓ between two sites on the fractal as the length of the shortest path connecting them. Figures 3 and 4 show that, as for linear fractals, the chemical distance ℓ (and not the Euclidean distance r) is the relevant physical length scale also for percolation clusters, such that the fluctuations of the probability density on sites with the same chemical distance ℓ from the origin are small. Figure 3 shows, for fixed ℓ and t, the histogram $N(\ln P)$ defined as the number of sites with probability $\ln P$ between $\ln P$ and $\ln P+d\ln P$, (a) for a large number $N_{\rm av}$ of configurations and (b) for a single configuration. In Fig. 4 the corresponding histograms for

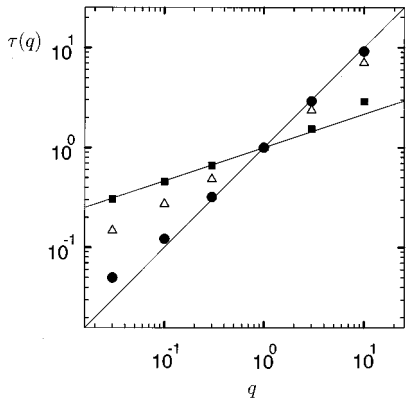

FIG. 2. Plot of $\tau(q)$ versus q for random walks on RW trails in the s.c. lattice at $t=5000$ and $r/R(t)\simeq 2.5$ for different $N_{\rm av}$ values [$N_{\rm av}=1$ (circles), $N_{\rm av}=10$ (triangles), and $N_{\rm av}=10^4$ (squares)]. The two lines in the plots represent the theoretical slopes 1 and 1/3.

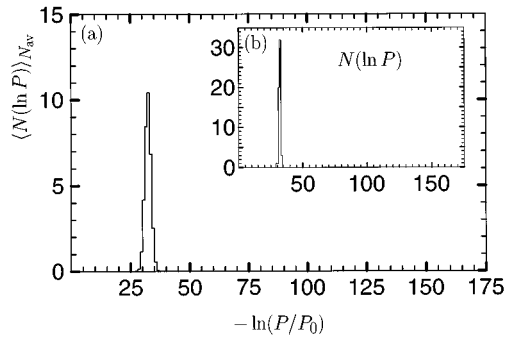

FIG. 3. Plot of the histogram $N(\ln P)$ versus $\ln(P/P_0)$ for percolation clusters in $d=2$ for fixed $\ell=100$ and $t=2000$, (a) averaged over 10^3 configurations and (b) for a single configuration.

fixed r are plotted. By comparing Figs. 3 and 4 it is clearly seen that the fluctuations at fixed chemical distance ℓ from the origin are considerably smaller than the fluctuations at fixed Euclidean distance r. Hence we can assume that approximately all sites i at fixed chemical distance ℓ from the origin have the same probability density $\langle P(\ell,t)\rangle$. In this approximation, we have trivially, as for RW trails,

$$\langle P_q(\ell,t)\rangle^{1/q}\sim\langle P(\ell,t)\rangle. \tag{20}$$

As predicted by scaling theory, $\langle P(\ell,t)\rangle$ scales as $\langle P(\ell,t)\rangle/\langle P(0,t)\rangle=f(\ell/L(t))$, where $L(t)$ is the mean chemical distance the random walker has traveled at time t (see Fig. 5). To test the validity of Eq. (20), we have calculated $\langle P_q(\ell,t)\rangle$ for various q and t values. The results (for percolation in $d=2,3$ and on the Cayley-tree) are shown in Fig. 6, where we have plotted $\langle P_q(\ell,t)\rangle^{1/q}$ versus $\ell/L(t)$ for fixed time and three q values. At large ℓ values, all data for different q collapse, while at smaller ℓ values slight deviations from (20) occur.

As can be seen from Fig. 5, at large ℓ values the slopes of the curves are consistent with the prediction $d_w/(d_w-d_{\min})$ by Havlin and Ben-Avraham [12]. At small values, however, the slopes are consistent with $d_w/d_{\min}$. The crossover occurs roughly at $L(t)$:

$$-\ln\langle P(\ell,t)\rangle\sim\begin{cases}(\ell/L(t))^{d_w/d_{\min}}, & \ell\ll L(t)\\ (\ell/L(t))^{d_w/(d_w-d_{\min})}, & \ell\gg L(t).\end{cases} \tag{21}$$

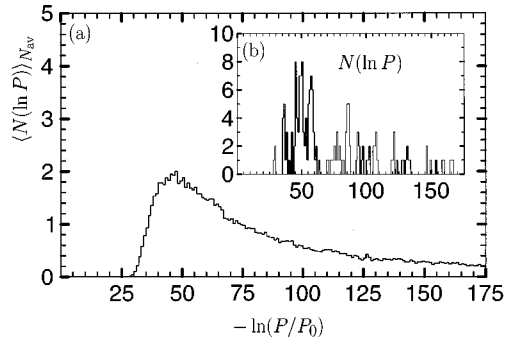

FIG. 4. Plot of the histogram $N(\ln P)$ versus $\ln(P/P_0)$ for percolation clusters in $d=2$ for fixed $r=70$ and $t=2000$ (a) averaged over 10^3 configurations and (b) for a single configuration.

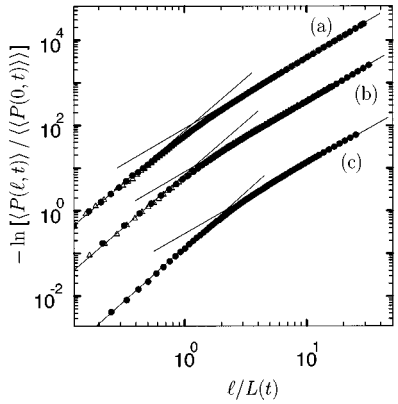

FIG. 5. Random walks on random fractals in the *chemical* space: Scaling plot of $-\ln[\langle P(\ell,t)\rangle/\langle P(0,t)\rangle]$ as a function of $\ell/L(t)$ for (a) percolation clusters in $d=2$ for $t=5000$ (circles) and $t=10\,000$ (triangles), (b) percolation clusters in $d=3$ for $t=1000$ (circles) and $t=5000$ (triangles), (c) for the Cayley-tree for $t=2000$ (circles) and $t=5000$ (triangles). The two lines in the plots represent the theoretical slopes with effective exponents d_w taken at the considered time instances. For clarity, the data in (a) and (b) have been multiplied by factors of 100 and 10, respectively.

This crossover behavior of $\langle P(\ell,t)\rangle$ has been overlooked in previous calculations of $\langle P(\ell,t)\rangle$. We would like to note that a similar crossover behavior has been observed earlier for random walks on the Sierpinski-gasket [13] where ℓ scales linearly with r.

Using the fact that the fluctuations of the probability density on sites i at fixed chemical distance ℓ from the origin of the random walk are small, for both the same and different configurations, $\langle P_q(r,t)\rangle$ can be written also for percolation clusters as a convolutional integral between $\langle P_q(\ell,t)\rangle$ and the probability $\phi(\ell|r)$ that two sites with Euclidean distance r are at chemical distance ℓ from each other (see also [4,10]),

$$\langle P_q(r,t)\rangle_{N_{\rm av}}=\int_{\ell_{\min}(r,N_{\rm av})}^{\infty}\phi(\ell|r)\langle P_q(\ell,t)\rangle d\ell, \tag{22}$$

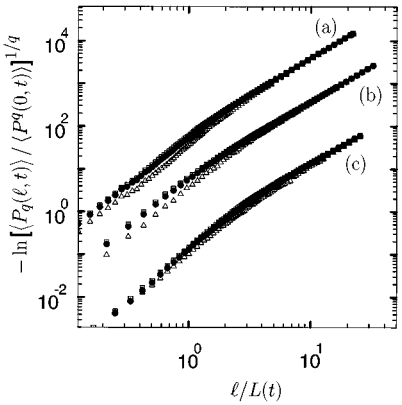

FIG. 6. Random walks on random fractals: Plot of $-\ln[\langle P_q(\ell,t)\rangle/\langle P^q(0,t)\rangle]^{1/q}$ as a function of $\ell/L(t)$ for several q values [$q=0.2$ (squares), $q=1$ (circles), and $q=4.0$ (triangles)] for (a) percolation clusters in $d=2$ at $t=2000$, (b) percolation clusters in $d=3$ at $t=1000$, and (c) for the Cayley-tree at $t=2000$. For clarity, the data in (a) and (b) have been multiplied by factors of 100 and 10, respectively.

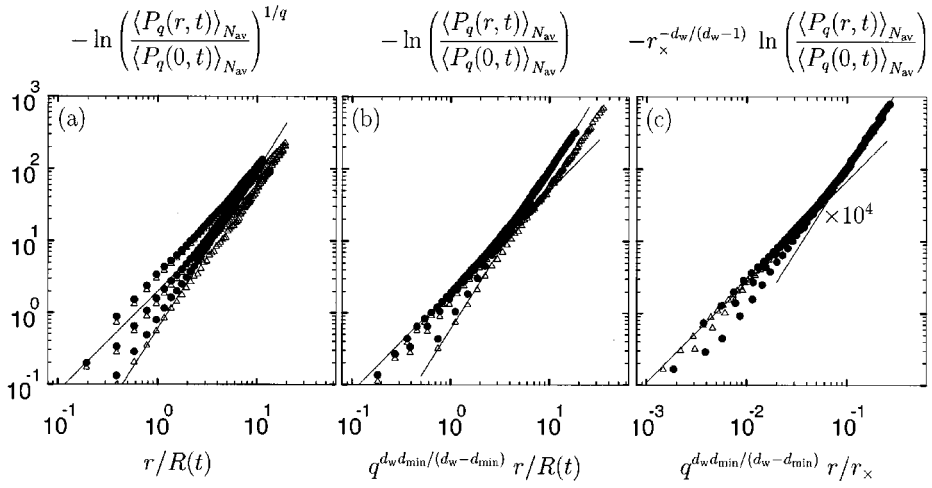

FIG. 7. The logarithm of the averaged moments of the probability density of random walks on percolation clusters in $d=3$ at $t=1000$ (a) as a function of $r/R(t)$, (b) as a function of $q^{d_w d_{\min}/(d_w-d_{\min})} r/R(t)$, and (c) as a function of $q^{d_w d_{\min}/(d_w-d_{\min})} r/r_\times(N_{\rm av})$ for $N_{\rm av}=1$ (circles) corresponding to the typical moment and $N_{\rm av}=125$ (triangles). Three different q values are plotted ($q=0.2$ [upper curve in (a)], $q=1$ [middle curve in (a)], and $q=4.0$ [lower curve in (a)]). The two lines in the plots represent the theoretical slopes with an effective exponent d_w taken at the considered time $t=1000$.

where now $\phi(\ell|r)$ is given by

$$\phi(\ell|r)=\frac{C_1}{\ell}\left(\frac{r}{\ell^{1/d_{\min}}}\right)^g \exp\left[-C_2\left(\frac{r}{\ell^{1/d_{\min}}}\right)^{\tilde\delta}\right] \tag{23}$$

with $\tilde\delta=d_{\min}/(d_{\min}-1)$ and $g\simeq 1.35$ in $d=2$, $g\simeq 1.5$ in $d=3$, respectively [14,15]. For fixed r, $\phi(\ell|r)$ has a maximum at $\ell_{\max}(r)\simeq r^{d_{\min}}$. Similar to RW trails [Eqs. (8) and (9)], the lower integration limit $\ell_{\min}(r,N_{\rm av})$ scales with the number $N_{\rm av}$ of configurations according to [10]

$$\ell_{\min}(r,N_{\rm av})\sim r_c(N_{\rm av})^{1-d_{\min}} r^{d_{\min}}, \tag{24}$$

for r above a crossover distance

$$r_c(N_{\rm av})=(\ln z+\ln N_{\rm av})/\ln(1/p_c). \tag{25}$$

Due to the crossover behavior of $\langle P(\ell,t)\rangle$ [Eq. (21)], a scaling relation for $\langle P_q(r,t)\rangle_{N_{\rm av}}$ can only be obtained in the limits $r\to 0$ and $r\to\infty$. For $r\to 0$, the ℓ values below $L(t)$ dominate the integral (22) [9], and therefore $\langle P^q(r,t)\rangle_{N_{\rm av}}$ satisfies the scaling relation

$$\langle P^q(r,t)\rangle_{N_{\rm av}}\sim\langle P(rq^{1/d_w},t)\rangle_{N_{\rm av}}. \tag{26}$$

For very large r values, on the other hand, only large ℓ values contribute, and thus

$$\langle P^q(r,t)\rangle_{N_{\rm av}}\sim\langle P(rq^{(d_w-d_{\min})/d_w d_{\min}},t)\rangle_{N_{\rm av}}. \tag{27}$$

By these scaling relations, the calculation of the moments again is reduced to a calculation of the first moment. The situation, however, is more complex than for the RW trail, since both scaling relations hold only in the limits of small and large r values and deviations from them are expected in the relevant r regime in between. In the asymptotic regime we have [10], in close analogy to (12) and (13),

$$-\ln\langle P(r,t)\rangle_{N_{\rm av}} \sim\begin{cases}[r/R(t)]^{d_w/(d_w-1)}, & R(t)\ll r\ll r_\times(N_{\rm av}),\\ r_c(N_{\rm av})^\alpha[r/R(t)]^{d_w d_{\min}/(d_w-d_{\min})}, & r\gg r_\times(N_{\rm av}),\end{cases} \tag{28}$$

with $\alpha=(d_{\min}-1)/(d_{\min}/d_w-1)$, $R(t)\sim L(t)^{d_{\min}}$, and the crossover length

$$r_\times(N_{\rm av})\simeq r_c^{(d_w-1)/d_w}(N_{\rm av})R(t). \tag{29}$$

For obtaining the moments we follow the procedure outlined in the foregoing section. As in Sec. II, we are only interested in the behavior in the asymptotic regime where the scaling relation (27) holds. Equations (27) and (28) can be written as $\langle P_q(r,t)\rangle_{N_{\rm av}}\sim\langle P(r,t)\rangle_{N_{\rm av}}^{\tau(q)}$, with

$$\tau(q)=\begin{cases}q^{(d_w/d_{\min}-1)/(d_w-1)}, & q_1\ll q\ll q_c(N_{\rm av}),\\ q, & q\gg q_c(N_{\rm av}),\end{cases} \tag{30}$$

and the crossover values

$$q_1\simeq[R(t)/r]^{d_w d_{\min}/(d_w-d_{\min})}$$

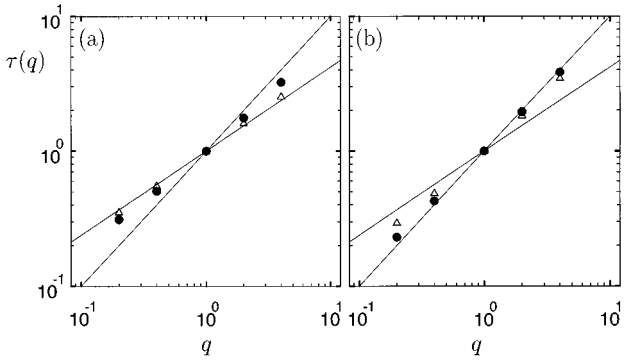

FIG. 8. Plot of $\tau(q)$ versus q for random walks on percolation clusters in $d=3$ for $t=1000$, $r/R(t)\simeq 3.5$ (a) and $r/R(t)\simeq 9$ (b) and different $N_{\rm av}$ values [$N_{\rm av}=1$ (circles) and $N_{\rm av}=125$ (triangles)]. The two lines represent the theoretical slopes with an effective exponent d_w taken at the considered time $t=1000$.

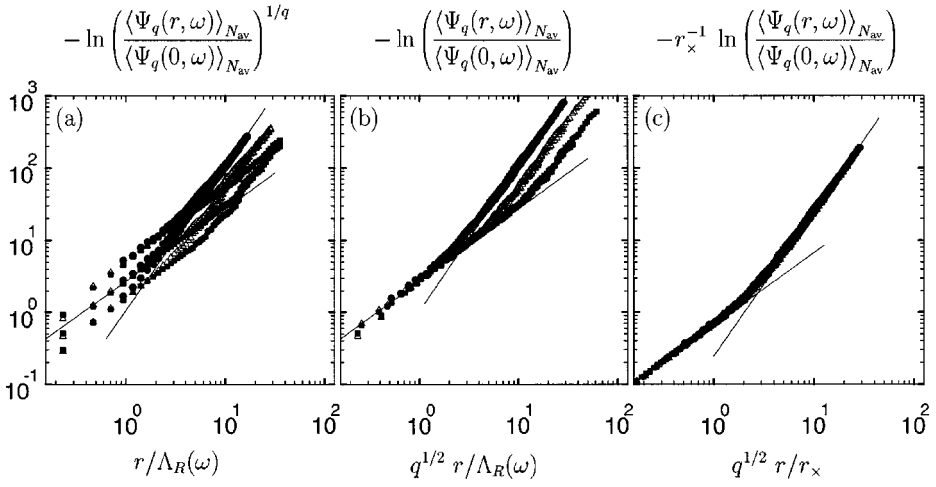

FIG. 9. The logarithm of the averaged moments of the amplitudes of localized vibrational excitations on RW trails in the s.c. lattice in appropriately scaled form for $\Lambda_\ell(\omega)\simeq 12$ (a) as a function of $r/\Lambda_R(\omega)$, (b) as a function of the single scaled variable $q^{1/2}r/\Lambda_R(\omega)$, and (c) as a function of the double scaled variable $q^{1/2}r/r_\times(N_{\rm av})$. The different symbols represent the numbers $N_{\rm av}$ of configurations in the averages [$N_{\rm av}=1$ (circles), $N_{\rm av}=10$ (triangles), and $N_{\rm av}=10^4$ (squares)]. For each $N_{\rm av}$ three different q values are plotted ($q=0.3$ [upper curve in (a)], $q=1$ [middle curve in (a)], and $q=3.0$ [lower curve in (a)]). The two lines in the plots represent the two theoretical slopes 1 and 2. For $N_{\rm av}$ below 10^4, averages have been performed over 1000 sets of $N_{\rm av}$ configurations (see also [11]).

and

$$q_c(N_{\rm av})\simeq r_c(N_{\rm av})^{(d_w-1)/(d_w/d_{\rm min}-1)}q_1.$$

Equation (30) predicts a similar behavior as for random walks on RW trails. Again there exists a critical q value $q_c(N_{\rm av})$ that increases logarithmically with $N_{\rm av}$. Below $q_c(N_{\rm av})$, we have multifractal behavior, above $q_c(N_{\rm av})$, we have unifractal behavior. In contrast to the situation on the RW trail, however, the multifractality does not vanish for the typical average ($N_{\rm av}=1$), since $r_c(1)>1$ here. Figures 7 and 8 show our numerical results for site percolation in $d=3$. In Fig. 7 the moments are plotted for $t=1000$ and three q and two $N_{\rm av}$ values in appropriately scaled form (a) as a function of $r/R(t)$, (b) as a function of $q^{d_w d_{\rm min}/(d_w-d_{\rm min})}r/R(t)$, and (c) as a function of $q^{d_w d_{\rm min}/(d_w-d_{\rm min})}r/r_\times(N_{\rm av})$. As for the RW trail, the results are in full quantitative agreement with the theory. Figure 8 shows $\tau(q)$ obtained from the moments at fixed r and t value for the typical average ($N_{\rm av}=1$) and for $N_{\rm av}=125$. The figure shows clearly the increase of the transition point $q_c(N_{\rm av})$ with $N_{\rm av}$, which separates the multifractal from the unifractal regime.

IV. LOCALIZED VIBRATIONAL EXCITATIONS IN RANDOM FRACTALS

First we discuss localized vibrational excitations in a linear random fractal. We consider a linear chain of masses M. Nearest neighbor masses are coupled by springs of force constants f. At a single site of the chain considered as the origin, a smaller mass $m=1<M$ is located. The masses perform longitudinal vibrations around their equilibrium positions. At frequency $\omega=\sqrt{(4f/M)}$ a localized excitation centered around the origin occurs. The displacements of the masses at chemical distance ℓ from the origin are given by (see, e.g., [16])

$$u(\ell)=u_0(-1)^\ell\Psi(\ell,\omega)\exp(-i\omega t), \tag{31}$$

where the normalized vibrational amplitudes decay as

$$\Psi(\ell,\omega)\sim\exp(-\ell/\Lambda_\ell(\omega)). \tag{32}$$

Next we consider that this chain forms a RW trail. We are interested in the behavior of $\langle\Psi(r,\omega)\rangle_{N_{\rm av}}$, averaged over $N_{\rm av}$ configurations and the corresponding moments $\langle\Psi_q(r,\omega)\rangle_{N_{\rm av}}$. The problem of finding $\langle\Psi_q(r,\omega)\rangle_{N_{\rm av}}$ is completely analogous to the problem of finding $\langle P_q(r,t)\rangle_{N_{\rm av}}$ on the RW trail. Replacing $P(\ell,t)$ in (3) by $\Psi(\ell,\omega)$ leads to the corresponding equation for $\langle\Psi_q(r,\omega)\rangle_{N_{\rm av}}$. It is easy to verify that Eq. (10) is now substituted by

$$\langle\Psi_q(r,\omega)\rangle_{N_{\rm av}}\sim\langle\Psi(rq^{1/2},\omega)\rangle_{N_{\rm av}}. \tag{33}$$

In full analogy to $\langle P(r,t)\rangle_{N_{\rm av}}$ [Eqs. (12) and (13)], the asymptotic regime of $\langle\Psi(r,\omega)\rangle_{N_{\rm av}}$ is split into two parts [8],

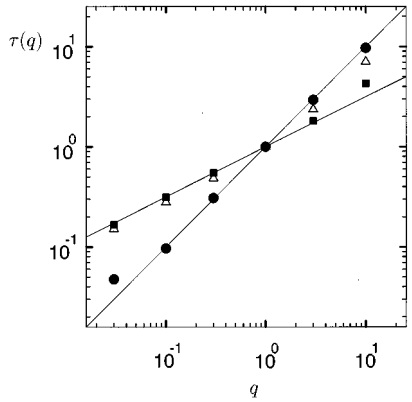

FIG. 10. Plot of $\tau(q)$ versus q for localized vibrational excitations on RW trails in the s.c. lattice for $\Lambda_\ell(\omega)\simeq 12$ and $r/\Lambda_R(\omega)\simeq 4$ for $N_{\rm av}=1$ (circles), $N_{\rm av}=10$ (triangles), and $N_{\rm av}=10^4$ (squares). The two lines in the plots represent the theoretical slopes 1 and 1/2.

$$-\ln\langle\Psi(r,\omega)\rangle_{N_{\rm av}} \sim \begin{cases} [r/\Lambda_R(\omega)], & \Lambda_R(\omega)\ll r\ll r_\times(N_{\rm av}) \\ r_c^{-1}(N_{\rm av})[r/\Lambda_R(\omega)]^2, & r\gg r_\times(N_{\rm av}), \end{cases} \tag{34}$$

with $\Lambda_R(\omega)=\sqrt{\Lambda_\ell(\omega)d/2}$, $r_\times(N_{\rm av})=\Lambda_R(\omega)r_c(N_{\rm av})$, and $r_c(N_{\rm av})$ from (9). Combining (33) and (34) we obtain $\langle\Psi_q(r,\omega)\rangle_{N_{\rm av}}\sim\langle\Psi(r,\omega)\rangle_{N_{\rm av}}^{\tau(q)}$, with

$$\tau(q)=\begin{cases} q^{1/2}, & q_1\ll q\ll q_c(N_{\rm av}), \\ q, & q\gg q_c(N_{\rm av}), \end{cases} \tag{35}$$

and the crossover values $q_1\simeq[\Lambda_R(\omega)/r]^2$ and $q_c(N_{\rm av})\simeq r_c(N_{\rm av})^2 q_1$.

Figures 9 and 10 show our numerical result for localized vibrational excitations on RW structures with a single defect, employing quadruple precision for the data. In Fig. 9 the moments in appropriately scaled form for $\Lambda_\ell(\omega)\simeq 12$ and several q and $N_{\rm av}$ values are plotted (a) as a function of $r/\Lambda_R(\omega)$, (b) as a function of the single scaled variable $q^{1/2}r/\Lambda_R(\omega)$, and (c) as a function of the double scaled variable $q^{1/2}r/r_\times(N_{\rm av})$. As for random walks on the RW trail, the results are in full quantitative agreement with the theory. Figure 10 shows $\tau(q)$ obtained from the moments at fixed r and $\Lambda_\ell(\omega)$ value for several values of $N_{\rm av}$. Again, for the typical average corresponding to $N_{\rm av}=1$, there exists only the unifractal region. For $N_{\rm av}\gg 1$, the transition point $q_c(N_{\rm av})$, separating the multifractal from the unifractal regime, is clearly seen and increases logarithmically with $N_{\rm av}$.

The considerations for the localized excitations on the RW trail can be extended straightforwardly to fractons on percolation clusters, if we *assume* (as has been done before by Bunde *et al.* [3]) that the fracton amplitudes are mainly determined by their chemical distances ℓ from the localization center and decay asymptotically as

$$\Psi(\ell,\omega)\sim\exp(-\ell/\Lambda_\ell(\omega)) \tag{36}$$

as in the RW trail. Using this striking assumption we can derive, as in the preceding sections before, a scaling relation between $\langle\Psi_q(r,\omega)\rangle_{N_{\rm av}}$ and $\langle\Psi(r,\omega)\rangle_{N_{\rm av}}$, which yields in the asymptotic regime of interest,

$$\tau(q)=\begin{cases} q^{1/d_{\rm min}}, & q_1\ll q\ll q_c(N_{\rm av}) \\ q, & q\gg q_c(N_{\rm av}), \end{cases} \tag{37}$$

with $q_1=[\Lambda_R(\omega)/r]^{d_{\rm min}}$ and $q_c(N_{\rm av})=r_c(N_{\rm av})^{d_{\rm min}}q_1$. Here, $\Lambda_R(\omega)\sim\Lambda_\ell(\omega)^{d_{\rm min}}$ represents the spatial localization length. As before, the critical q value $q_c(N_{\rm av})$ separating the multifractal from the unifractal regime increases logarithmically with $N_{\rm av}$. In the limit of $N_{\rm av}\to\infty$ tends $q_c(N_{\rm av})\to\infty$, and only the multifractal regime remains. For $N_{\rm av}=1$, corresponding to the typical average, $q_c(N_{\rm av})$ has the minimum value. The numerical observation of $q_c(N_{\rm av})$, however, even for $N_{\rm av}=1$, is a difficult numerical task since in order to detect it unambigously (in $d=2$), distances of the order of 10 localization lengths from the localization center must be considered.

ACKNOWLEDGMENTS

We thank M. Porto for useful discussions. This work has been supported by the Deutsche Forschungsgemeinschaft.

[1] T. Brandes, L. Schweitzer, and B. Kramer, Phys. Rev. Lett. **72**, 3582 (1994).
[2] B. Huckestein, B. Kramer, and L. Schweitzer, Surf. Sci. **263**, 125 (1992).
[3] A. Bunde, H.E. Roman, St. Russ, A. Aharony, and A.B. Harris, Phys. Rev. Lett. **69**, 3189 (1992).
[4] A. Bunde, S. Havlin, and H.E. Roman, Phys. Rev. A **42**, 6274 (1990).
[5] L. de Arcangelis, S. Redner, and A. Coniglio, Phys. Rev. B **31**, 4725 (1985).
[6] *Fractals and Disordered Systems*, 2nd ed., edited by A. Bunde and S. Havlin (Springer, Heidelberg, 1996).
[7] *Fractals in Science*, edited by A. Bunde and S. Havlin (Springer, Heidelberg, 1994).
[8] A. Bunde and J. Dräger, Physica A **202**, 371 (1994).
[9] J. Dräger, St. Russ, and A. Bunde, Europhys. Lett. **31**, 425 (1995).
[10] A. Bunde and J. Dräger, Phys. Rev. E **52**, 53 (1995).
[11] The concept of the typical average $\langle P(r,t)\rangle_{\rm typ}$ can be easily extended to typical averages over $N_{\rm av}$ configurations, which are obtained by first averaging over the $P(r,t)$ of the $N_{\rm av}$ configurations yielding $\langle P(r,t)\rangle_{N_{\rm av}}$ and then averaging $\ln\langle P(r,t)\rangle_{N_{\rm av}}$ over all sets of $N_{\rm av}$ configurations.
[12] S. Havlin and D. Ben Avraham, Adv. Phys. **36**, 695 (1987).
[13] S. Havlin, R. Nossal, B. L. Trus, G. H. Weiss, Phys. Rev. A **45**, 7511 (1992); J. Klafter, G. Zumofen, and A. Blumen, J. Phys. A **24**, 4835 (1991).
[14] U.A. Neumann and S. Havlin, J. Stat. Phys. **52**, 203 (1988).
[15] A. Bunde and J. Dräger, Philos. Mag. B **71**, 721 (1995).
[16] C. Kittel, *Introduction to Solid State Physics* (Wiley, New York, 1967).